



SPE-121097-PP

Navier-Stokes Simulations of Surface Waves Generated by Submarine Landslides: Effect of Slide Geometry and Turbulence

Debashis Basu, Steve Green, Kaushik Das, Ron Janetzke, and John Stamatakos, Southwest Research Institute®, 6220 Culebra Road, San Antonio, TX 78238, USA

Copyright 2009, Society of Petroleum Engineers

This paper was prepared for presentation at the 2009 SPE Americas E&P Environmental & Safety Conference held in San Antonio, Texas, USA, 23–25 March 2009.

This paper was selected for presentation by an SPE program committee following review of information contained in an abstract submitted by the author(s). Contents of the paper have not been reviewed by the Society of Petroleum Engineers and are subject to correction by the author(s). The material does not necessarily reflect any position of the Society of Petroleum Engineers, its officers, or members. Electronic reproduction, distribution, or storage of any part of this paper without the written consent of the Society of Petroleum Engineers is prohibited. Permission to reproduce in print is restricted to an abstract of not more than 300 words; illustrations may not be copied. The abstract must contain conspicuous acknowledgment of SPE copyright.

Abstract

Surface waves generated by submarine landslides are studied using a computational model based on Navier-Stokes equations. The volume of fluid (VOF) method is used to track the free surface and shoreline movements. A Renormalization Group (RNG) turbulence model and Detached Eddy Simulation (DES) multiscale model are used to simulate turbulence dissipation. The submarine landslide is simulated using a sliding mass. The three-dimensional numerical simulations are carried out for a freely falling wedge representing the landslide and subsequent wave generations. Simulation results are compared with the experimental data. Modeled illustrate the effect of slide geometry, computational grid, turbulence model parameters, and slide material density on the predicted wave characteristics and runup/rundown at various locations. Computed results also show the complex three-dimensional flow patterns in terms of the velocity field, shoreline evolution, and free-surface profiles. Predicted numerical results for time histories of free-surface fluctuations and the runup/rundown at various locations are in good agreement with the available experimental data.

Introduction

Tsunamis are typically generated by co-seismic sea bottom displacement due to earthquakes. However, submarine or subaerial landslides can also trigger devastating tsunamis. Submarine landslides, which often accompany large earthquakes, can disturb the overlying water column as sediment and rock slump down slope. Any type of geophysical mass flow including debris flows, debris avalanches, landslides, and rockfalls can generate submarine-landslide-generated tsunamis. These types of tsunamis can produce large runup heights that flood the coast (Masson et al. 2006). While the mechanisms that generate these types of tsunami flows are generally understood, the ability to predict the flows they produce at coastlines still represents a formidable challenge due to the complexities of coastline formations and the presence of numerous coastal structures that interact and alter the flow. Furthermore, landslide-generated tsunamis can present significant risks to offshore structures, such as oil and gas production platforms and remote terminal facilities. Tsunami hazards posed by submarine landslides depend on the landslide scale, location, type, and process. Even small submarine landslides can be dangerous when they occur in coastal areas. Examples include the 1996 Finneidfjord slide (Longva et al. 2003) and the 1929 Grand Banks earthquake that resulted in submarine landslides, turbidity current, and a tsunami that caused significant casualties (Fine et al. 2005; Masson et al. 2006; Piper et al. 1999). Although the generation and propagation of earthquake-generated tsunamis have been studied for the last four decades and are now relatively well understood, the causes and effects of landslide-generated tsunamis are much less known. The generation and effects of landslide-generated tsunamis are complex and variable. Historical landslide-generated tsunamis have produced locally extreme wave heights of hundreds of meters, as exemplified by the greater than 100-foot wave heights in Lituya Bay, Alaska, that were generated by the 1958 Lituya Bay landslide (Miller 1960).

Theoretical approaches for solving the landslide-generated tsunami problems are difficult to apply due to strong nonlinearities of equations that govern tsunami behaviors, the three-dimensionality of the flow, and the turbulence that develops from breaking waves of tsunami. Depth-averaged techniques, including Boussinesq models (Lynett et al. 2002), do not predict the flowfield details accurately. Recent advances in computational fluid dynamics (CFD) have made it possible to use CFD techniques for investigation of tsunami runup. However, three-dimensional simulations of tsunami wave propagation are very difficult due to the complexity, the physical scales of the flow regimes, and the presence of the free surface. Grilli et al. (2002) used three-dimensional boundary element numerical models to predict the initial propagation of

the surface disturbance. The Eulerian formulation is widely used to simulate tsunami flows, because it is relatively easy to implement the conservation laws of motion. Prior simulations of landslide-generated tsunamis (Liu et al. 2005; Grilli and Watts 1999; Lynett and Liu 2005; Rzedkiewicz et al. 1997) used models based on Navier-Stokes equations. These analyses (Liu et al. 2005; Grilli and Watts 1999; Lynett and Liu 2005; Rzedkiewicz et al. 1997) either used two-dimensional Navier-Stokes simulations with a VOF-type free surface tracking or a multifluid finite element-based Navier-Stokes model (Rzedkiewicz et al. 1997) in which air and water motion were simulated. Most of these simulations were carried out in a two-dimensional framework and the results were quite promising. Gisler et al. (2003, 2006) carried out full three-dimensional Navier-Stokes analysis of tsunami generation and propagation, but that was computationally very expensive. Liu et al. (2005) used Eulerian grid-based Large Eddy Simulation (LES) technique to study the waves and runup/rundown generated by three-dimensional sliding mass. Christensen and Deigaard (2001) and Lin and Liu (1998a, 1998b) used RANS models to simulate breaking waves in a surf zone. While most of the prior simulations focused on prediction of the impulse wave characteristics, none of them looked into the effect of slide geometry, turbulence, and grid resolution on the predicted wave characteristics and run-up. Najafi-Jilani and Ataie-Ashtiani (2008) carried out experimental studies to evaluate the influence of slide geometry, initial submergence, and bed slope.

The present investigation aims at evaluating the effect of slide geometry and the effect of turbulence models on the impulse wave characteristics and runup/rundown at various locations. In the present work, the Navier-Stokes equations are used to predict the submarine landslide movement and the subsequent generation and propagation of tsunami waves. Three-dimensional simulations are carried out for the Navier-Stokes equations; the flow solver FLOW-3D (Flow Sciences 2006) is used. FLOW-3D uses the VOF method to track the free surface and shoreline movement. Three different types of slide geometry have been assessed: a triangular wedge-shaped slide, an ellipsoidal geometry slide, and a rectangular slide. Turbulence is simulated using both the RNG-based turbulence model (Yakhot and Smith 1992) and the multiscale DES model (Basu 2006). The DES model is implemented in the FLOW-3D solver and is based on the RNG-based turbulence model. The effect of the turbulence model (baseline RNG turbulence model and RNG-based DES model) on the flowfield is investigated. The current simulations use the experimental data of Heinrich (1992). The computational geometry and the experimental data are obtained from the work of Heinrich (1992) and Ataie-Ashtiani and Shobeeyri (2008). Numerical results from the simulations are compared with experimental data (Heinrich 1992; Ataie-Ashtiani and Shobeeyri 2008) for the time histories of free-surface fluctuations and the runup/rundown at various locations. The three-dimensionality of the flowfield is illustrated through iso-surfaces of vorticity and coherence function.

Solver Methodology

FLOW-3D (Flow Sciences 2006), is a general purpose CFD simulation software package based on the algorithms for simulating fluid flow that were developed at Los Alamos National Laboratory in the 1960s and 1970s (Hirt and Nichols 1981; Harlow and Welch 1965; Welch et al. 1966). The basis of the solver is a finite volume or finite difference formulation, in Eulerian framework, of the equations describing the conservation of mass, momentum, and energy in a fluid. The code is capable of simulating two-fluid problems, incompressible and compressible flow, and laminar and turbulent flows. The code has many auxiliary models for simulating phase change, non-Newtonian fluids, non-inertial reference frames, porous media flows, surface tension effects, and thermo-elastic behavior. FLOW-3D solves the fully three-dimensional transient Navier-Stokes equations using the Fractional Area/Volume Obstacle Representation (FAVOR) (Hirt and Sicilian 1985) and the volume of fraction (Hirt and Nichols 1981) method. The solver uses finite difference or finite volume approximation to discretize the computational domain. Most of the terms in the equations are evaluated using the current time-level values of the local variables in an explicit fashion, though a number of implicit options are available. The pressure and velocity are coupled implicitly by using the time-advanced pressures in the momentum equations and the time-advanced velocities in the continuity equations. It solves these semi-implicit equations iteratively using relaxation techniques. FAVOR (Hirt and Sicilian 1985) defines solid boundaries within the Eulerian grid and determines fractions of areas and volumes (open to flow) in partially blocked volume to compute flows correspondent to those boundaries. In this way, boundaries and obstacles are defined independently of grid generation, avoiding saw-tooth representation or the use of body-fitted grids. FLOW-3D has a variety of turbulence models for simulating turbulent flows, including the Prandtl mixing length model, one-equation model and two-equation k - ϵ model, RNG scheme, and an LES model. The current simulations use the RNG model (Yakhot and Smith 1992). In addition, a multiscale DES turbulence model (Basu 2006) was implemented in FLOW-3D. Both the turbulence models are compared for their relative performance.

RNG Turbulence Model

The RNG turbulence model solves for the turbulent kinetic energy (k) and the turbulent kinetic energy dissipation rate (ϵ). This RNG approach applies statistical methods to derive the averaged equations for turbulent quantities, such as turbulent kinetic energy (k) and its dissipation rate. The RNG-based models rely less on empirical constants while setting a framework to derive a range of parameters to be used at different turbulence scales. The RNG model uses equations similar to the

equations for the k- ϵ model. However, equation constants that are found empirically in the standard k- ϵ model are derived explicitly in the RNG model. Generally, the model has wider applicability than the standard k- ϵ one.

DES Multiscale Turbulence Model

The DES modeling approach differs from the RANS modeling approach by the eddy diffusivity closure. While the RANS closure models model the entire spectrum of turbulence, the DES variants allow some of the turbulence to be resolved explicitly, reducing the dependence on modeling. The DES formulations allow the reduction of eddy viscosity in the regions of interest, and fine scales are resolved. A switching function is used to activate the reduction in eddy viscosity. For the present simulations, a RNG-based DES multiscale turbulence model (Basu, 2006) is implemented in FLOW-3D. The model is detailed in Basu (2006). In the DES model used, the switching function depends on both the local grid length and the turbulent length scale. A model constant C_b is also used to modify the eddy viscosity formulation. The effect of this model constant C_b on the flowfield is also explored.

Experimental Work

The experiment was done by Heinrich (Heinrich 1992). The experiments were carried out in a channel that was 20 m long, 0.55 m wide, and 1.50 m deep in the Hydraulic National Laboratory, Chatou, France (Heinrich 1992). In this experiment, water waves were generated by allowing a wedge to freely slide down a plane inclined at 45° on the horizontal. The wedge was triangular in cross section (0.5×0.5 m) with a 2000 kg/m³ density. The water depth was 1 m, and the top of the edge was initially 1 cm below the horizontal free surface. The box was equipped with four rollers, slid into the water under the influence of gravity only, and was abruptly stopped as it reached the bottom by a 5-cm-high rubber buffer. The box was held in its initial position by a hydraulic jack moving laterally through the unglazed side wall.

Computational Details

The experiment described by Heinrich (1992) was conducted in a wave tank that approximated a two-dimensional flowfield. In these simulations, both two- and three-dimensional representations were used so that the presence of even moderate three-dimensional effects could be investigated and compared to the two-dimensional simulations and the experiments. A three-dimensional flow domain representing the experiment setup described by Ashtiani et al. (Ataie-Ashtiani 2008) and Heinrich (1992) was defined within the framework of the FLOW-3D software. The entire flow domain, shown in **Fig. 1**, is 4.1 m in length and 1.2 m in height. For the three-dimensional grids, a width of 1 m was assumed for the wave tank. The blocks representing the landslide were assumed to be 0.8 m wide and centered in the tank. The ramp in these experiments has a 1:1 slope, and the wedge is placed so that its top face is submerged 0.1 m below the water surface. Likewise, the ellipse and the rectangular block were placed such that uppermost extent of each was 1 cm below the water surface. The water depth is specified as 1.0 m. The initial fluid configuration for the different slide geometries is shown in **Fig. 2**. The coordinate system for these simulations has its origin at the bottom of the flow channel directly below the location where the water surface meets the water level. Uniform grids were used for all simulations. A baseline mesh of 120×40×40 cells in the x-, y-, and z-directions, respectively, was defined for these simulations. In addition, for the mesh resolution studies, coarser and finer meshes were specified with 0.701 and 1.414 times the resolution of the baseline mesh. Note that the grid also covers the initial air space above the water to accommodate the block motion and the surface waves. This feature is required in the FLOW-3D software as part of its VOF free-surface tracking algorithm.

All surfaces of the flow domain were defined as no-slip smooth walls. Similarly, the faces of the wedge and ramp were also smooth no-slip surfaces. The wedge motion follows the prescribed velocity profile Ashtiani et al. (2008) specified. This velocity profile is a piecewise linear fit to the following function

$$V(t)=86 \tanh(0.0175t), t \leq 0.4s \quad (1)$$

$$V(t)=0.6 \quad t > 0.4s \quad (2)$$

where the velocity units are m/s. The prescribed time history of the wedge speed is described in **Fig. 3**. Note that the velocity profile is nearly linear during the block acceleration. In these simulations, the block was decelerated to a stop between $t=1.4$ s and $t=1.45$ s so that it rested at the bottom of the ramp. The fluid in the channel was specified as water with a density of 1000 kg/m³ and a viscosity of 1 centipoise. In the experiments described by Ashtiani et al. (2008), air filled the space above the water. In these simulations, however, this was empty space that did not interact with the water. Laminar flow conditions prevail over most of the flow domain except near the moving edge. The baseline case for these simulations was to use the robust multiscale DES version of the RNG turbulence model developed by Basu (2006). This was used for most of the simulations described here. For comparison purposes, a standard RNG turbulence model was used for the three-dimensional simulation of the wedge motions. Finally, again for comparison purposes, a laminar-only condition for the two-dimensional simulations of the wedge motion was also used.

Results and Discussions

Computational results are presented for the Navier-Stokes simulations, and the simulated results are compared with the experimental data. Presented results include the unsteady fluid configurations at different times and comparison of the predicted water surface height and elevation with experimental observations. The effect of slide geometry and the turbulence model constants on the predicted solution are also shown.

Figs. 4a, 4b, and 4c present the unsteady flowfield. All three figures show the velocity vectors overlaid on contours of total effective (*i.e.*, laminar + turbulent) dynamic viscosity. All of these figures are taken from the simulation using the multiscale DES turbulence model with the turbulence parameter $C_b=0.3$. Fig. 4a shows the initial wave at the time $t=0.5$ s when the trough behind the wave is about at its minimum position. There is significant turbulence in the flow behind the wedge as shown by an effective dynamic viscosity about 10 times the fluid molecular viscosity. In Fig. 4b, at $t=1.0$ s, the runup wave is at its maximum position on the ramp and the second wave is just beginning to propagate. Note that the entire portion of the wake behind the wedge is in turbulent flow. Finally, Fig. 4c shows the flow at the time $t=2.0$ s when the second wave is propagating down the channel just above the block. Note that the vortex that was formerly behind the top corner of the block has detached from the block over time and two counter-rotating vortices are moving away from the block.

The fluid surface shapes predicted by the various simulations are compared at time $t=1.0$ s in **Fig. 5**. The predictions for the time history of the wave runup behind the block are shown in **Fig. 6**. The two-dimensional simulation and experimental results shown in Fig. 6 are in relatively good agreement. All of the three-dimensional simulations, however, exhibit varying amounts of runup along the ramp depending on the shape of the block. Note that the curves for all three different levels of grid resolution simulations of the wedge motion are in very close agreement. This demonstrates that the grid used here is sufficiently fine to capture the pertinent fluid dynamics. Likewise, the curves for the three different turbulence models used in the simulations of the wedge motion are also in close agreement. This shows that the turbulence model constant details do not strongly affect the overall motion of the fluid. Figs. 5 and 6 show that the shape of the slide creating the fluid motion significantly impacts the wave shape and runup.

The effect of the slide shape and geometry on the overall flow structure and turbulence is shown in **Fig. 7**. The effect of wedge geometry on the overall fluid turbulence is seen by comparing Figs. 7a, 7b and 7c. Fig. 7a shows the effective dynamic viscosity for the rectangular block at a time of $t=1.0$ s, Fig. 7b shows the corresponding view for the ellipsoidal block, and Fig. 7c shows the corresponding view for the triangular wedge shape. The rectangular block and the triangular wedge have approximately the same levels of effective viscosity; however, the ellipsoidal block has an overall lower value of effective viscosity. This is because the ellipsoid has a more hydrodynamically efficient shape than the two more bluff shapes of the other two blocks. The separation and the separation region is more pronounced for the rectangular block and the triangular block; hence the level of eddy viscosity is also higher for the rectangular and triangular slide.

The effect of the DES turbulence model constant on the flowfield and eddy viscosity is shown in **Fig. 8**. Fig. 8a shows the effective dynamic viscosity from the DES model with parameter $C_b=0.1$ for the triangular block at a time of $t=1.0$ s; Fig. 8b shows the corresponding view of effective dynamic viscosity for $C_b=0.5$. Note that the effective dynamic viscosity is higher for $C_b=0.5$ compared to $C_b=0.1$. The higher values of effective dynamic viscosity can be observed in the near wall and wake regions. In the far-field region, the values of the effective dynamic viscosity are nearly the same for both C_b values. It is evident that lowering the value of C_b decreases the eddy viscosity in the shear layer and wake region. This is inherent in the DES formulation (Basu 2006). By reducing the value of C_b , the effective grid-length scale also gets reduced, and consequently, the eddy viscosity is also reduced. For transonic cavity flow, Hamed et al. (2007) observed a similar reduction of eddy viscosity with lower values of C_b that also enables the model to resolve fine-scale structures.

The three-dimensional nature of the surface wave and the runup are shown in **Fig. 9** at time $t=1.0$ s for the triangular block. This figure shows that even for a moving block that spans most (but not all) of the width of the flow channel, there are pronounced three-dimensional effects. The wave front is convex, and there is a pronounced variability in the shape of the wave that runs up the ramp behind the moving block. The flow turbulence is highly localized near the moving block and dictates how this local flowfield interacts with the block. **Fig. 10** shows an isosurface of the coherence function, $Q=0.2$, around the block. There are significant structures associated with the vortices trailing from the two sides of the block. There is a third structure associated with the vortex trailing from the top edge of the block that gives rise to the high effective viscosity area shown in Figs. 4b and 4c.

Conclusions

Three-dimensional Navier-Stokes simulations were carried out to model tsunami wave generation by submarine landslides. Computed results are compared with available experimental data. Simulated results show that the flow is strongly three-dimensional and turbulent. The three-dimensionality of the flow is evident even though the landslide fills over 50 percent of the width of the flow domain. This suggests that very few realistic landslide events can be modeled accurately with two-

dimensional simulations. Different sizes and shapes of the slide were used to analyze the influence of the slide shape on the flowfield. Computed results showed that slides with hydrodynamically efficient shapes produce less turbulence and bluff body effect. The DES turbulence model constant seems to influence the eddy viscosity. Lower values of the model constant results in a lower value of eddy viscosity. The flow turbulence is found to be localized. The details of the flow turbulence do not greatly affect the far field effects such as wave height and runup. In the near field, however, turbulence appears to play a stronger role. Accurate prediction of turbulence may be more important in determining how the landslide material spreads after the event and results in the post-event damage to coastal areas and offshore structures. These risk assessments were outside the scope of this investigation. However, the computational tool developed for prediction of landslide-generated tsunamis during this investigation has great application to oil and gas industries, especially for oil exploration regions and offshore structures. The application of this developed computational tool can help provide inputs to assess risk from landslide-generated tsunamis for near shore as well as offshore structures.

Acknowledgments

The work was sponsored by the Advisory Committee for Research at Southwest Research Institute® through an Internal Research and Development Project. The authors acknowledge the useful discussions provided by the technical support staff from Flow Sciences, Inc., and the help from Sharon Odum at the Geosciences and Engineering Division in preparing the manuscript.

References

- Ataie-Ashtiani, B. and Shobeyri, G. 2008. Numerical Simulation of Landslide Impulsive Waves by Incompressible Smoothed Particle Hydrodynamics. *International Journal of Numerical Methods in Fluids* **56**: 209–232.
- Basu, D. 2006. Hybrid Methodologies for Multiscale Separated Turbulent Flow Simulations. PhD Dissertation, University of Cincinnati, Cincinnati, Ohio.
- Christensen, E.D. and Deigaard, R. 2001. Large Eddy Simulation of Breaking Waves. *Coastal Engineering* **42**: 53–86.
- Flow Sciences Incorporated. 2006. Flow-3D Users Manual, Version 9.1. Santa Fe, NM: Flow Sciences Incorporated.
- Fine, I.V., Rabinovich, A.B., Bornhold, B.D., Thomson, R.E., and Kulikov, E.A. 2005. The Grand Banks Landslide-Generated Tsunami of November 18, 1929: Preliminary Analysis and Numerical Modeling. *Marine Geology* **203**: 201–218.
- Gisler, G., Weaver, R., Mader, C., and Gittings, M.L. 2003. Two- and Three-Dimensional Simulations of Asteroid Ocean Impacts. *Science of Tsunami Hazards* **21** (2): 119–134.
- Gisler, G., Weaver, R., and Gittings, M.L. 2006. SAGE Calculations of the Tsunami Threat From La Palma. *Science of Tsunami Hazards* **24** (4): 288–301.
- Grilli, S.T., Vogelmann S., and Watts, P. 2002. Development of a 3D Numerical Wave Tank for Modeling Tsunami Generation by Underwater Landslides. *Engineering Analysis with Boundary Elements* **26** (4): 301–313.
- Grilli, S.T. and Watts, P., 1999. Modeling of Waves Generated by a Moving Submerged Body, Applications to Underwater Landslides. *Engineering Analysis with Boundary Elements* **23**: 645–656.
- Hamed, A., Basu, D., and Das, K., 2007. Assessment of Multiscale Resolution for Hybrid Turbulence Model in Unsteady Separated Transonic Flows. *Computers and Fluids* **36** (5): 924–934.
- Harlow, F.H. and Welch, J.E. 1965. Numerical Calculation of Time-Dependent Viscous Incompressible Flow. *Physics of Fluid* **8**: 2182–2189.
- Heinrich, P. 1992. Nonlinear Water Waves Generated by Submarine and Aerial Landslides. *Journal of Waterway, Port, Coastal and Ocean Engineering* **118** (3): 249–266.
- Hirt, C.W. and Nichols, B.D. 1981. Volume of Fluid (VOF) Method for the Dynamics of Free Boundaries. *Journal of Computational Physics* **39**: 201–225.
- Hirt, C.W. and Sicilian, J.M. 1985. A Porosity Technique for the Definition of Obstacles in Rectangular Cell Meshes. *Proc., Fourth International Conference on Ship Hydrodynamics*, Washington, DC, National Academy of Sciences, 1–19.
- Lin, P. and Liu, P.L.-F. 1998a. A Numerical Study of Breaking Waves in the Surf Zone. *Journal of Fluid Mechanics* **359**: 239–264.
- Lin, P. and Liu, P.L.-F. 1998b. Turbulence Transport, Vortices Dynamics, and Solute Mixing Under Plunging Breaking Waves in Surf Zone. *Journal of Geophysical Research* **103** (C8): 15677–15694.

- Liu, P.L.-F., Wu, T.-R., Raichlen, F., Synolakis, C.E., and Borrero, J.C. 2005. Runup and Rundown Generated by Three-Dimensional Sliding Masses. *Journal of Fluid Mechanics* **536**: 107–144.
- Longva, O., Janbu, N., Blikra, L.H., and Boe, R. 2003. The Finneidfjord Slide: Seafloor Failure and Slide Dynamic. In *Submarine Mass Movements and Their Consequences*, ed. J. Locat and J. Mienert, 531–538. Dordrecht, Netherlands: Kluwer Academic Publishers.
- Lynett, P., Wu, T.-R., and Liu, P.L.-F. 2002. Modeling Wave Runup with Depth Integrated Equations. *Coastal Engineering* **46** (2): 89–107.
- Lynett, P. and Liu, P.L.-F. 2005. A Numerical Study of the Runup Generated by Three-Dimensional Landslides. *Journal of Geophysical Research* **110** (03006): doi:10.1029/2004JC002443.
- Masson, D.G., Harbitz, C.B., Wynn, R.B., Pedersen, G., and Lovholt, F. 2006. Submarine Landslides: Processes, Triggers and Hazard Prediction. *Philosophical Transaction of the Royal Society* **364**: 2009–2039.
- Miller, D.J. 1960. Giant Waves in Lituya Bay, Alaska. Geological Survey Professional Paper 354-C, U.S. Government Printing Office, Washington, DC.
- Najafi-Jilani, A. and Ataie-Ashtiani, B. 2008. Estimation of Near-Field Characteristics of Tsunami Generation by Submarine Landslide. *Ocean Engineering* **35** (5–6): 545–557.
- Piper, D.J.W., Cochonat, P., and Morrison, M.L. 1999. The Sequence of Events Around the Epicenter of the 1929 Grand Banks Earthquake: Initiation of Debris Flows and Turbidity Currents Inferred From Sidescan Sonar. *Sedimentology* **46**: 79–97.
- Rzadkiewicz, A.S., Mariotti, C., and Heinrich, P. 1997. Numerical Simulation of Submarine Landslides and Their Hydraulic Effects. *Journal of Waterway, Port, Coastal, and Ocean Engineering* **123** (4): 149–157.
- Welch, J.E., Harlow, F.H., Shannon, J.P., and Daly, B.J. 1966. The MAC Method: A Computing Technique for Solving Viscous, Incompressible, Transient Fluid Flow Problems Involving Free-Surfaces. Los Alamos Scientific Laboratory Report LA-3425.
- Yakhot, V. and Smith, L.M. 1992. The Renormalization Group, the e-Expansion and Derivation of Turbulence Models. *Journal of Scientific Computing* (7): 35–61.

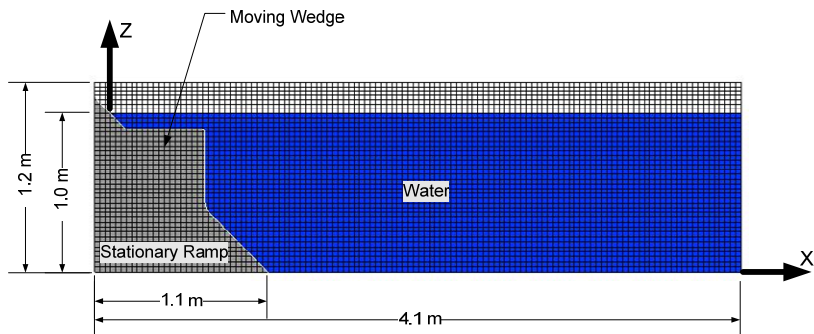


Fig. 1–Flow domain and initial fluid configuration used in the simulations for the experimental data of Heinrich (1992)

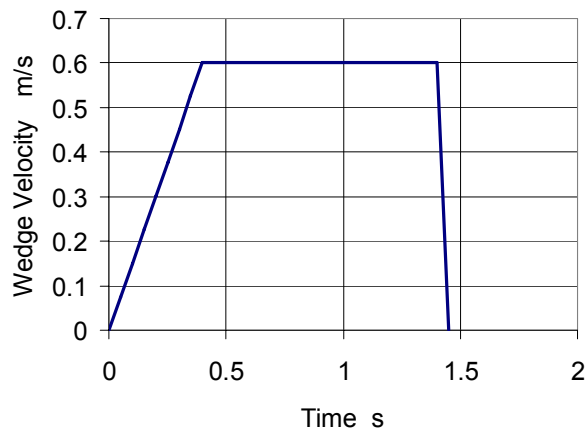
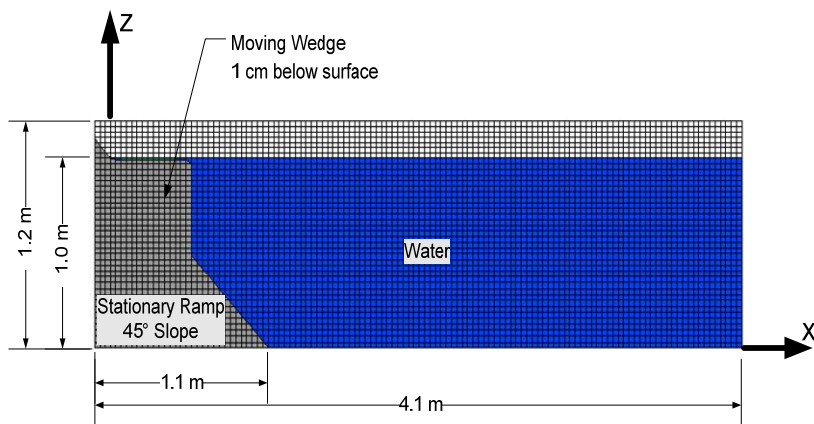


Fig. 3–Prescribed time history of the wedge speed for the experimental data of Heinrich (1992)

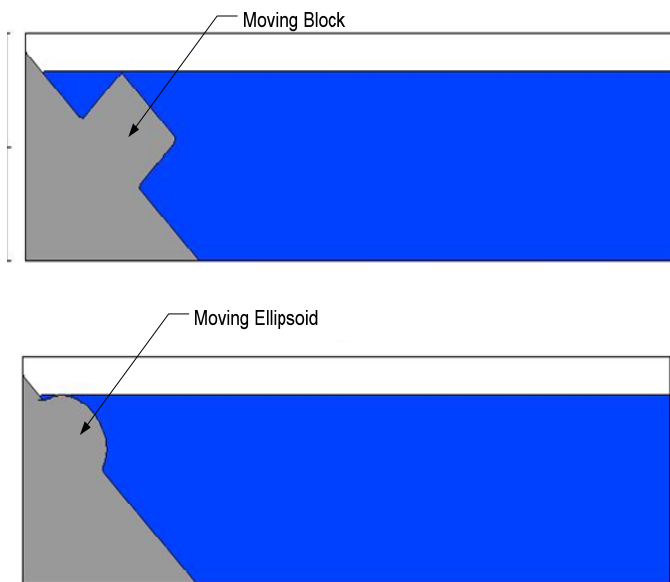


Fig. 2–Initial fluid configurations for different shapes of slides

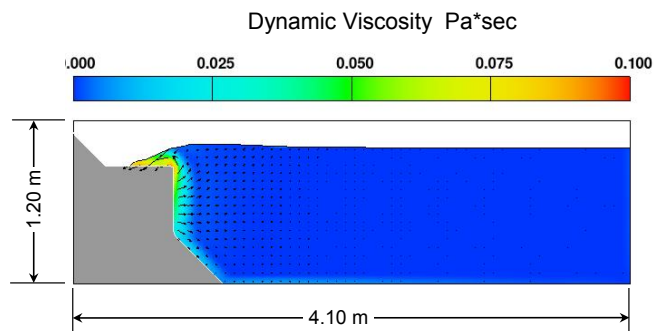


Fig. 4a–Fluid configuration at t=0.5 sec; minimum trough behind wedge=1

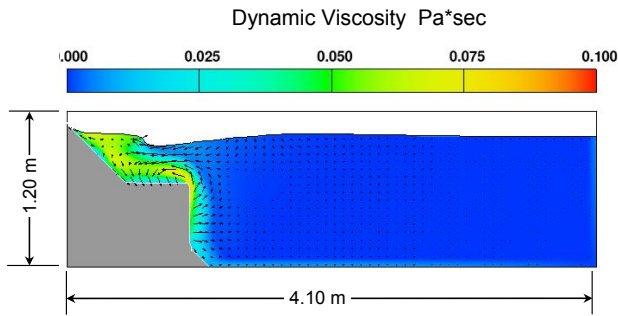


Fig. 4b—Fluid configuration at $t=1.0$ sec;
the second wave is generated

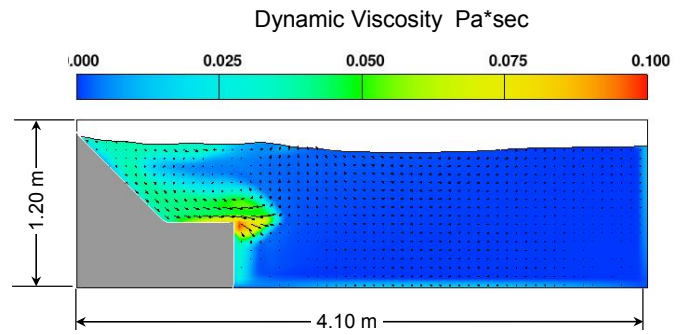


Fig. 4c—Fluid configuration at $t=2.0$ sec;
wedge stopped, second wave propagating

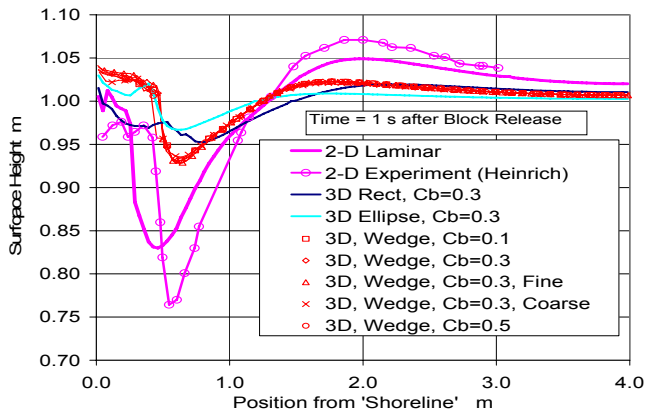


Fig. 5—Comparison of fluid surface profiles

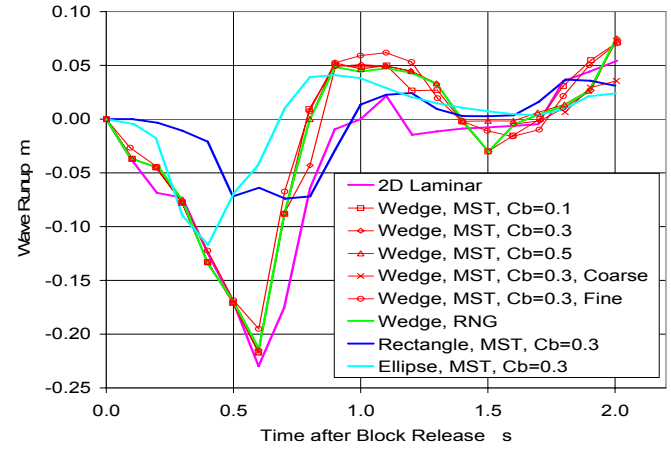
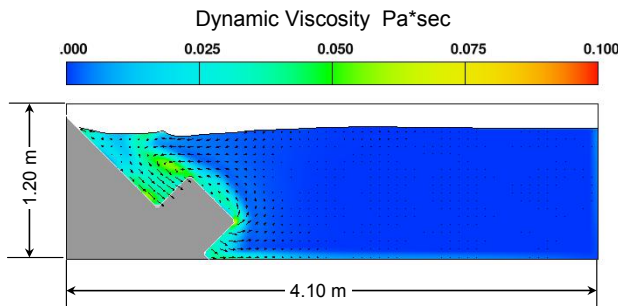
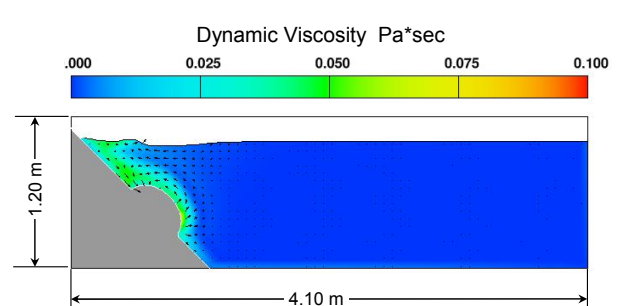


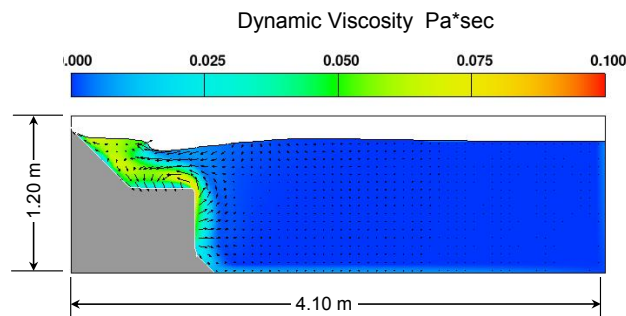
Fig. 6—Comparison of wave runup behind block



(7a) Rectangular Slide



(7b) Elliptical Slide



(7c) Triangular Wedge Slide

Fig. 7—Fluid configurations for different slide geometries

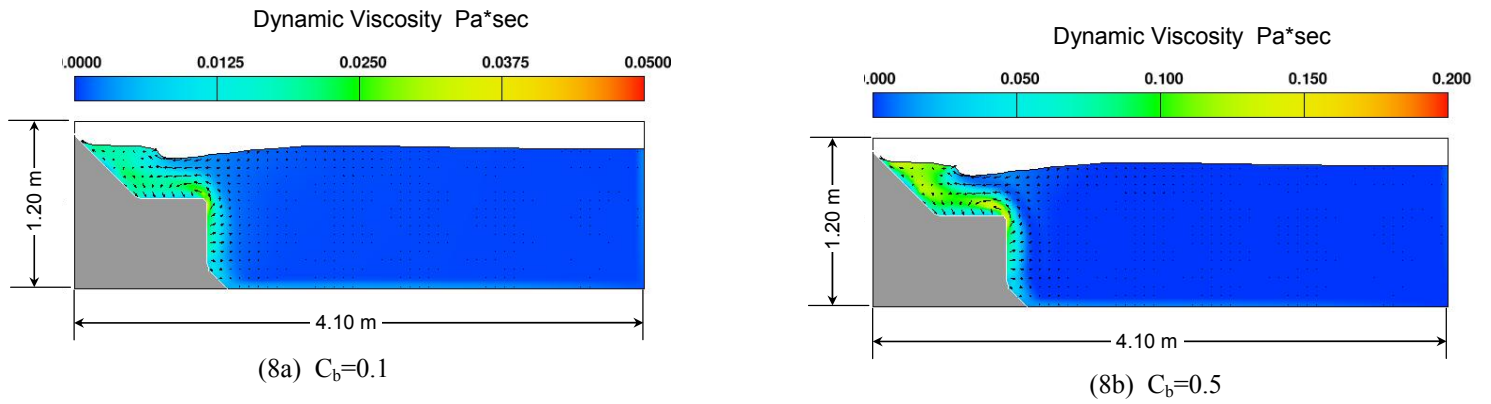


Fig. 8—Fluid configuration for different turbulence model constants

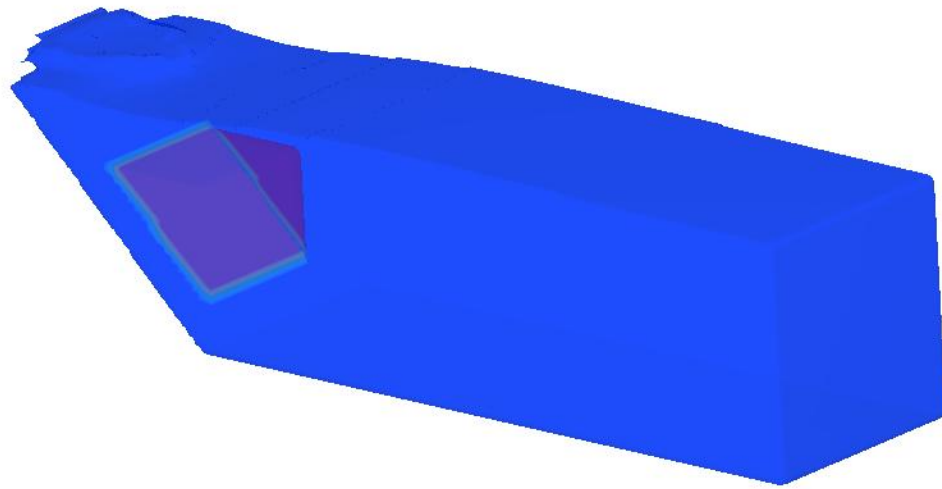


Fig. 9—Three-dimensional fluid surface at $t=1.0$ s for wedge block

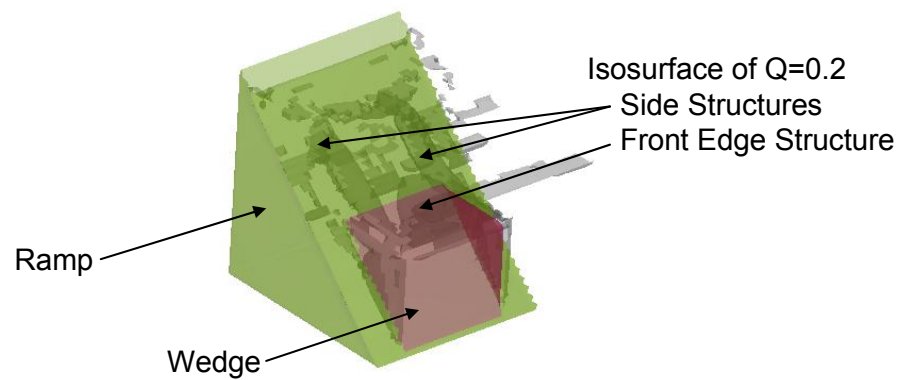


Fig. 10—Isosurfaces of Q at $t=1.0$ s for wedge block showing the turbulence structures